

Coupling of Surface Chemistry and Electric Double Layer at TiO_2 Electrochemical Interfaces

Chao Zhang,^{*,†} Jürg Hutter,[‡] and Michiel Sprk[¶]

[†]*Department of Chemistry-Ångström Laboratory, Uppsala University, Lägerhyddsvägen 1, BOX 538, 75121, Uppsala, Sweden*

[‡]*Institut für Chemie, Universität Zürich, Winterthurerstrasse 190, CH-8057 Zürich, Switzerland*

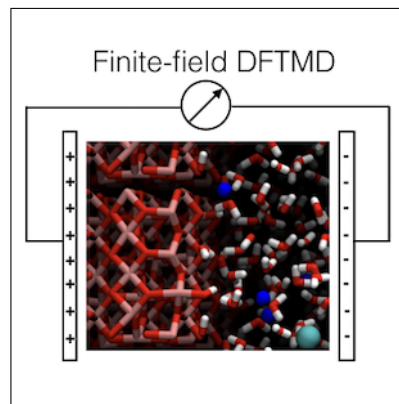
[¶]*Department of Chemistry, University of Cambridge, Lensfield Rd, Cambridge CB2 1EW, United Kingdom*

E-mail: chao.zhang@kemi.uu.se

Abstract

Surfaces of metal oxides at working conditions are usually electrified due to the acid-base chemistry. The charged interface compensated with counterions forms the so-called electric double layer. The coupling of surface chemistry and electric double layer is considered to be crucial but poorly understood because of lacking the information at the atomistic scale. Here, we used the latest development in density functional theory based finite-field molecular dynamics simulation to investigate pH-dependence of the Helmholtz capacitance at electrified rutile TiO_2 (110)-NaCl electrolyte interfaces. It is found that, due to competing forces from surface adsorption and from electric double layer, water molecules have a stronger structural fluctuation at high pH and this leads to a much larger capacitance. It is also seen that, interfacial proton transfers at low pH increase significantly the capacitance value. These findings elucidate the microscopic origin for the same trend observed in titration experiments.

Graphical TOC Entry



The surface chemistry of metal oxides is more involved than that of metals because the surface charge depends on proton exchange driven by pH of the environment.^{1,2} The condition in which the surface has no net proton charge is called the point of zero proton charge (PZPC).³⁻⁵ However, working conditions for most earth-abundant metal oxide based photocatalysts are not at PZPC and the corresponding solid-liquid interface is highly electrified.⁶ By attracting counterions from the solution side, the electric double layer (EDL) is formed at the interface in which the electric field can be as high as 10^9 V/m.⁷ Therefore, including the coupling of surface chemistry and EDL at metal oxide-electrolyte interfaces is necessary.

The differential capacitance C_{EDL} of the EDL at oxide materials-electrolyte interfaces has been long regarded as a key probe of its structure. For semiconducting oxides, the capacitance can be resolved into three distinct components connected in series:^{8,9}

$$1/C_{\text{EDL}} = 1/C_{\text{SC}} + 1/C_{\text{H}} + 1/C_{\text{GC}} \quad (1)$$

The first component is the result of the depletion or accumulation of electrons in the space charge (SC) layer of the semiconductor electrode, which can be 10 to 100 nm thick. The second component C_{H} is the Helmholtz capacitance due to specific adsorption of hydroxide groups or protons and corresponding counter ions. The last component C_{GC} called the Gouy-Chapman capacitance, stems from the diffusive electrolyte and depends on the ionic strength.

The relationship between surface structure and ion complexation of oxide-solution interface is a long-standing topic in colloid chemistry. Experimental interest in these metal oxide systems dates back to early 60s.^{10,11} In titration experiments, the variation of surface charges due to adsorption/desorption of H^+ is measured against the pH in solution. To interpret experiments, 2-pK model including a phenomenological neutral site (SOH^0), dissociate site (SO^-) and associate site (SOH_2^+) was introduced ("S" for the surface).¹² However, the structural information was completely over-

looked there until the development of surface complexation model in 1989.^{13,14} In the multi-site complexation (MUSIC) model and other types of bond valence model,^{15,16} proton affinity (or pKa) is correlated with the Pauling bond valance charge (the charge of a cation divided by its coordination number) and the Me-H distance. To connect with titration experiments, a Gouy-Chapman-Stern type EDL model was adopted to match the surface charges q and the potential generated from surface complexation models $\Delta\phi$. Thus, the capacitance C_{H} in surface complexation models is a (global) fitting parameter to titration experiments.^{17,18}

A more subtle yet important aspect is that proton affinity itself depends on the capacitance of EDL. Indeed, in the original paper of surface complexation model, authors subtracted Nernstian EDL contribution to pKa of the solution monomers but neglected it for the surface protonation reactions.¹³ This was inevitable because the dielectric constant of bulk water is well known as 78 in ambient conditions while the dielectric constant of EDL at oxide-electrolyte interfaces remains a puzzle.¹⁹

In parallel to the development by colloid chemists, electrochemists have their own interests in electrified metal oxide-electrolyte interfaces. Since the discovery of the Honda-Fujishima effect in 1972 for TiO_2 ,²⁰ metal oxide photo-electrochemistry attracts the perennial interest in water splitting research using solar energy. The focus there was to identify metal oxides having the right band alignment with respect to the water redox potential, for example, the conduction band minimum should be higher than the H^+/H_2 reduction potential.^{8,9,21} Over the years, experimental characterizations have moved from ultra-high vacuum condition to solid-liquid interface due to the advancement in surface science techniques.²²⁻²⁶

As for colloid chemists, the potential distribution at TiO_2 aqueous electrolyte interfaces also interested electrochemists. From the slope of Mott-Schottky plots, the Helmholtz capacitance as a function of pH was determined.²⁷ Despite that the reported median Helmholtz capacitance as $50 \mu\text{F}/\text{cm}^2$ is surprisingly close to the well-quoted value of $64 \mu\text{F}/\text{cm}^2$ by

colloid chemists,²⁸ opposite trends in its pH-dependence were seen.^{27,29}

Similar to the approximation colloid chemists took in building surface complexation model, the standard Pourbaix diagram in electrochemistry neglects the non-Nernstian contribution of EDL to the proton affinity.^{30,31} Therefore, elucidating the microscopic origin for the pH-dependence of Helmholtz capacitance and quantifying its contribution to the surface pKa is a common challenge in both fields.

Density functional theory based molecular dynamics (DFTMD) is a suitable technique to tackle this challenge which encompasses the electronic, structural and dynamical ingredients on an equal footing. DFTMD modeling of solid-liquid interface has been applied to different areas, such as studying the structure of water (defects) at solid interfaces,^{32–38} spectroscopic modeling of surface-sensitive vibrational signals,^{39–41} computing the surface acidity^{42–45} and determining the redox potential.^{46–49}

In spite of progress, electric properties, such as the dielectric constant and the interfacial capacitance which are at the heart of modeling the electrified solid-liquid interface, were usually thought to be beyond the reach of DFTMD. Thanks to the development of constant electric displacement \bar{D} Hamiltonian for the modeling of ferroelectric nanocapacitors by Vanderbilt and co-workers,⁵⁰ electric properties became more accessible to DFTMD simulations.^{51–56} We are therefore in a position to apply the hybrid constant \bar{D} simulation with PBE functional⁵⁷ to the charged rutile TiO₂ (110)-NaCl electrolyte interface as implemented in CP2K.^{58,59} In Eq. 1, C_{SC} is the smallest of three capacitances and will normally dominate in the inverse sum. However, its effect and associated depletion layer can be eliminated at the flatband potential condition by an appropriate bias potential.^{8,30} At the high ionic strength which is relevant for photoelectrocatalysis, the diffuse ionic layer has a higher capacitance and the inverse C_{GC} term can therefore be ignored. Based on these considerations, modeling the Helmholtz capacitance C_H is what we focus on in this work.

Conventionally, the Helmholtz capacitance

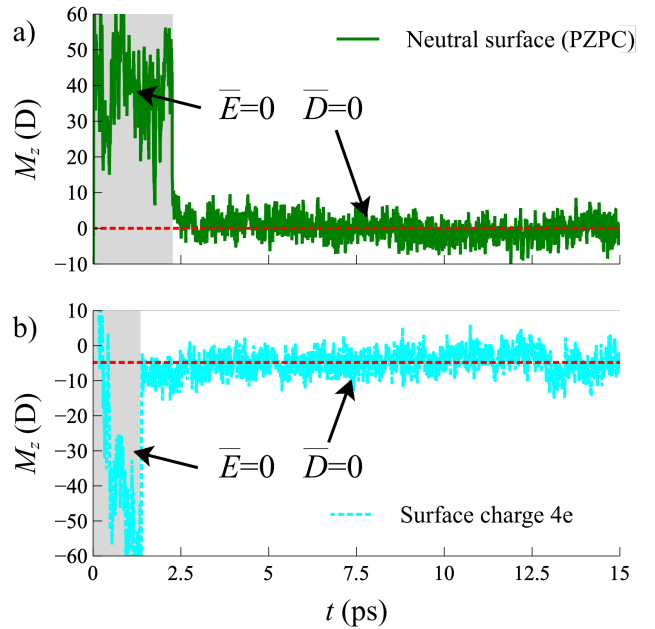


Figure 1: a) The time evolution of total dipole moment M_z at PZPC when switching electric boundary condition from $\bar{E} = 0$ to $\bar{D} = 0$; b) The time evolution of total dipole moment M_z with surface charge $4e$ when switching electric boundary condition from $\bar{E} = 0$ to $\bar{D} = 0$. Dash lines are the time average of M_z in each case.

can be computed as $C_H = q/\Delta\phi$ according to the textbook definition, where q is the surface charge and $\Delta\phi$ is the potential drop crossing the Helmholtz layer.^{60,61} Instead, by exploring the modern theory of polarization and constant \bar{D} method developed by Vanderbilt and co-worker for treating ferroelectric nanocapacitors,⁵⁰ we reformulated this problem in terms of the macroscopic polarization P_z of the system.⁵³ In our setup, the two sides of the oxide material can be charged at fixed chemical composition of the supercell by bearing same amount but opposite types of proton charges. This scheme leads to a succinct expression of the average Helmholtz capacitance C_H based on the supercell polarization P_z :⁵³

$$C_H = \left(\frac{\partial q}{2\pi L_z A \partial \langle P_z \rangle} \right)_{\bar{D}} \quad (2)$$

where L_z is the dimension of the model system perpendicular to the interface, q is the imposed proton charge, A is the area of the x, y cross

section and $\langle \dots \rangle$ indicates the ensemble average. The advantage of this formulation is three-fold. First, it does not require additional vacuum slab in the modeling as commonly used in surface science^{62,63} and the oxide is treated as one piece of material. Second, it removes the finite-size dependence of the oxide slab which plagues the computation of the Helmholtz capacitance.⁵³ Third, by switching the electric boundary condition to constant \bar{D} , the relaxation of P_z is significantly accelerated as predicted by the Debye theory of dielectrics.^{51,52}

When the oxide surface is charged by protonation or deprotonation, P_z deviates from zero in response. Therefore, P_z has to be zero at the PZPC and this serves as a critical test for the convergence of DFTMD simulations.⁶⁴ As shown in Fig. 1, at the PZPC, M_z relaxes to zero rapidly when switching the boundary condition from $\bar{E} = 0$ to $\bar{D} = 0$. Within 10 picoseconds, its time average is about 0.02 D. For the case of electrified interface with surface charge of $4e$, M_z turns out to be -4.76 D within a similar time-scale. In all cases, classical MD simulations were leveraged to pre-equilibrate the system before applying the hybrid constant \bar{D} DFTMD simulations.^{55,56}

Table 1: The averaged Helmholtz capacitance C_H , protonic Helmholtz capacitances C_H^+ and deprotonic Helmholtz capacitance C_H^- at different surface charge q . For $q = 2e$, the corresponding surface charge density for the supercell size used here is about $20 \mu\text{C}/\text{cm}^2$.

q	C_H ($\mu\text{F}/\text{cm}^2$)	C_H^+ ($\mu\text{F}/\text{cm}^2$)	C_H^- ($\mu\text{F}/\text{cm}^2$)
$2e$	81	67	101
$4e$	72	59	85

Simulation results of the average Helmholtz capacitance C_H at the rutile TiO_2 (110)- NaCl interface are shown in Table 1. Following Eq. 2, one obtains the average Helmholtz capacitance C_H which is about $76 \mu\text{F}/\text{cm}^2$. Although starting from very different initial configurations, C_H at surface charge $q = 2e$ and $q = 4e$ are in excellent agreement with each other. In order to decompose the overall Helmholtz capacitance into protonic C_H^+ and deprotonic C_H^- ,

we resorted to the macroscopic averaging technique^{59,65} and monitored the shift of the macro-averaged electrostatic potential with respect to the PZPC for the protonic side (Fig. 2 inset). From this decomposition, we found that C_H^- is about 50% higher than C_H^+ . At surface charge $q = 2e$ (about $20 \mu\text{C}/\text{cm}^2$ for the supercell used here⁵⁹), the surface potential for the deprotonic side is about 200 mV and that for the protonic side is about 300 mV, which can be measured in principle using the surface-sensitive vibrational spectroscopy⁶⁶ or the binding energy shift in X-ray photoelectron spectroscopy.⁶⁷

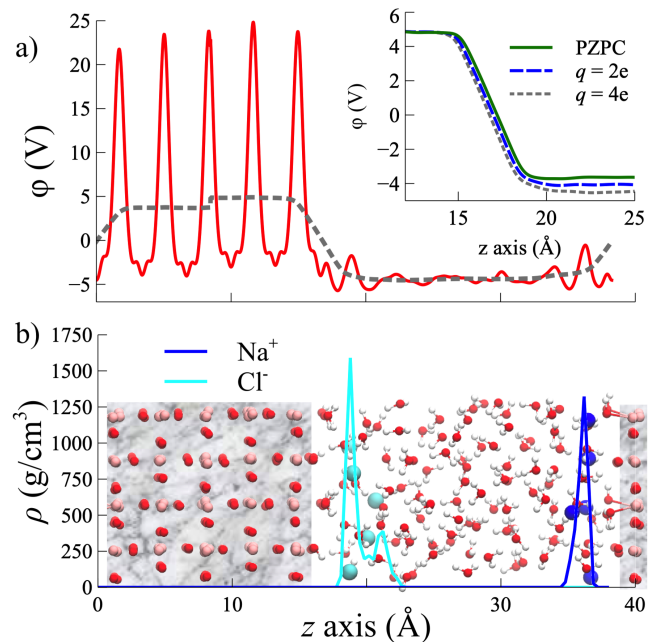


Figure 2: a) The planar averaged (solid line) and macro-averaged (dash line) electrostatic potential ϕ at surface charge $q = 4e$. Inset: Macro-averaged electrostatic potential for the protonic side at different surface charge densities; b) The corresponding density profiles of ions at surface charge $q = 4e$ overlaid with one snapshot of the model system. The protonic side is formed by adding extra H^+ to the oxygen sites and the deprotonic side is formed by removing H^+ from the absorbed water molecules. Thus, the supercell composition is kept fixed at different surface charge densities.

The range of experimental estimated capacitance for rutile TiO_2 - NaCl electrolyte goes from 64 to $160 \mu\text{F}/\text{cm}^2$.^{28,29,68} The scattered data reflect the nature of the observed capacitance

which depends on ionic strength and surface roughness.⁶⁹ In particular, the asymmetric pH-dependence (a higher Helmholtz capacitance at high pH) that we observed from DFTMD simulations is in accord with titration experiments of rutile at higher ionic strength^{29,70,71} and has been also seen in other metal oxides, such as ZnO.⁷²

The Stern layer width (the charge separation distance) for the negatively charged TiO₂ surface is about 2Å in our simulations (Fig. 2b) and this leads to an estimation of the interfacial dielectric constant of about 23. This number can be compared with the commonly assumed value of 26 for rutile TiO₂ in geochemistry and colloid science.⁷³ On the other hand, we found the Stern layer width for the positively charge TiO₂ surface is about the same ($\sim 2\text{\AA}$, Fig. 2b), thus the smaller capacitance of the protonic side C_H^+ (Table 1) suggests an interfacial dielectric constant of 15 instead. It is worth noting that the maxima in the radial distribution functions of Na⁺-O_w and Cl⁻-H_w in bulk salt solutions are 2.4Å and 2.9Å respectively with the PBE functional.⁷⁴ Therefore, the asymmetry of the interfacial capacitances found here should largely come from the difference in the dielectric screening at the interface.

At the PZPC condition, water molecules are adsorbed to the rutile TiO₂ (110) surface as dimers.⁷⁵ This is evidenced by the angular distribution of water dipole moments with respect to the normal vector of the surface (Fig. 3a). Water dipole moment preferably points out towards the electrolyte solution with primary and secondary peaks at 48° and 75°. For the positively charged side, the electric field of EDL enhances this pattern by shifting primary peak and secondary peaks to 33° and 48° respectively. The splitting between the two peaks becomes narrower and the overall distribution is less broad in comparison with the neutral surface. The situation is reversed for the negatively charged side. The angular distribution spans almost the whole range of possible values with primary and secondary peaks around 89° and 60°.

The much wider angular distribution of water molecules at the negatively charged side comes

from two competing factors: chemisorption of water molecules at rutile (110) would orientate water dipole towards to the electrolyte while the electric field in EDL tends to flip it. Indeed, adsorption and desorption can happen dynamically at the negatively charged side in contrast to the positively charged side because of this competition, as seen in Fig. 3b. Since the extent of dielectric screening is proportional to the magnitude of dipole moment fluctuation as formulated in Kirkwood-Onsager theory,^{52,76} it is not a surprise that we found the interfacial dielectric constant at the deprotonic side (therefore C_H^-) is much higher than that of protonic one.

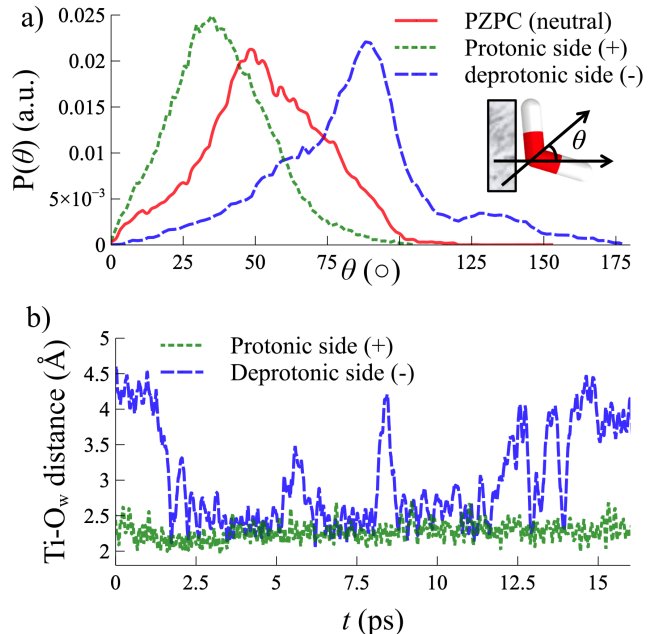


Figure 3: a) Probability distribution of the angle θ between water dipole moment and surface normal for neutral, positively and negatively charged ($q = 2e$) rutile TiO₂ (110)-electrolyte interfaces ; b) Dynamics of adsorbed water molecules at positively and negatively charged ($q = 2e$) rutile TiO₂ (110)-electrolyte interfaces.

This dynamical adsorption-desorption process of water molecules observed at the negatively charged side may play a role for the alternative mechanism of O₂ production in alkaline solution (high pH),⁷⁷ since adsorbed water molecules at the TiO₂ surface not only provide the raw material for OH· production but may

also block surface sites.²²

The dissociative adsorption of water molecules at the bare rutile TiO_2 (110) surface was extensively discussed in literature.^{32–34} Indeed, this is also observed for the neutral surface mediated by the neighboring water molecule (Ref.³⁶ and Fig. 4 a). One would expect the electric field due to the EDL will magnify this effect. However, instead of the dissociative adsorption, the hydrolysis of adsorbed water molecules releases ions to the electrolyte solution. In our simulations, this dominantly happens for the positively charged rutile TiO_2 (110) surface (Fig. 4 b), in accord with a much higher electric field generated in the protonic side.

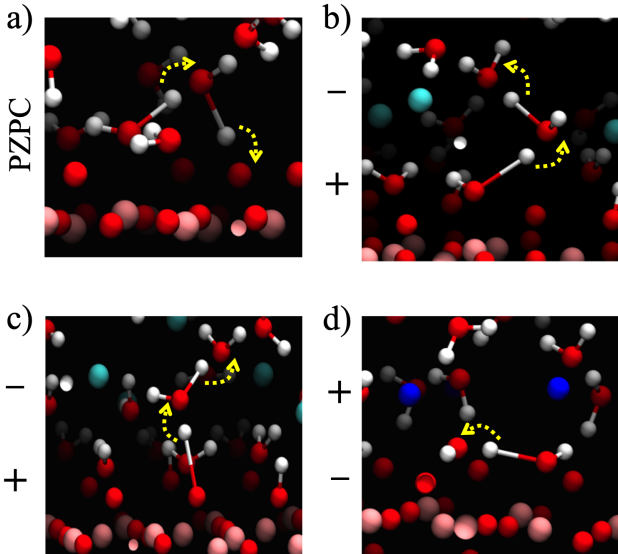


Figure 4: a) Dissociative adsorption of water molecules at the neutral surface (PZPC); b) Hydrolysis of adsorbed water molecules at the positively charged surface; c) Proton transfer between charged surface groups Ti_2OH^+ and solvating water molecules at the positively charged surface. Ti_2O indicates the bridging oxygens; d) Resonance between charged surface groups TiOH^- and adsorbed water molecules at the negatively charged side. TiOH^- stand for the hydroxylated 5-fold coordinated Ti groups.

The pK_a of the protonic rutile TiO_2 (110) was determined to be about -1.0 in DFTMD.⁴² Therefore, the estimated reaction free energy

for the proton transfer between the charged surface groups Ti_2OH^+ and solvating water molecules is comparable to thermal fluctuation energy at room temperature. Indeed, spontaneous proton exchange between them was observed for the protonic side of rutile TiO_2 (110), as shown in Fig. 4 c. On the contrary, the exchange of OH^- between TiOH^- and solvating water molecules is endothermic and no corresponding OH^- transfer event was observed at the deprotonic side. Instead, the resonance of charged group TiOH^- and surface groups with adsorbed water molecules TiH_2O happens (Fig. 4 d).

To quantify the effect of surface acid-base chemistry on the Helmholtz capacitance, we also carried out additional simulations by constraining adsorbed water molecules and charged surface groups Ti_2OH^+ to not undergo reaction. When only constraining adsorbed water molecules, the average Helmholtz capacitance C_H at $q = 4e$ turns out to be about $80\mu\text{F}/\text{cm}^2$. This value is very similar to the one about $72\mu\text{F}/\text{cm}^2$ in Table 1 without constraints. However, when both adsorbed water molecules and charged surface groups are constrained, C_H becomes about $44\mu\text{F}/\text{cm}^2$ which is close to results obtained previously.⁶¹ This significant reduction of capacitance can be understood, because the proton exchange between Ti_2OH^+ and solvating water molecules will shorten the charge separation distance in the EDL. Therefore, the surface acidity of the oxide is another determining factor for the Helmholtz capacitance.

In summary, using finite-field DFTMD simulations, we discovered the microscopic origin for the pH-dependent of Helmholtz capacitance at rutile TiO_2 (110) seen in titration experiments. At high pH, water molecules have a stronger structural fluctuation and this lead to a much larger capacitance. At low pH, proton transfer increases the capacitance value by reducing the charge separation distance. These observations for rutile TiO_2 (110) and the finite-field DFTMD modeling approach presented in this study pave the way to investigate electrochemical reactivity at electrified metal oxide-electrolyte interfaces, e.g. the Non-Nernstian contribution of the capacitance to the Pourbaix

diagram and the hole trapping in alkaline solutions.

Acknowledgement CZ thanks Deutsche Forschungsgemeinschaft (DFG) for a research fellowship (No. ZH 477/1-1) during his stay in Cambridge. CZ is grateful to Uppsala University for a start-up grant and to Åforsk Foundation for a research grant (Ref. nr. 18-460). Funding from the Swedish National Strategic e-Science program eSENCE is also gratefully acknowledged. Computational resources were provided by the UK Car-Parrinello (UKCP) consortium funded by the Engineering and Physical Sciences Research Council (EPSRC) of the United Kingdom. CZ also thanks J. Cheng for helpful discussions and T. Sayer for reading the manuscript.

Supporting Information Available

The following files are available free of charge.

The hybrid constant \bar{D} Hamiltonian and its corresponding CP2K input syntax. The details of CP2K simulations of electrified rutile TiO₂ (110)-NaCl electrolyte interfaces.

References

- (1) Ardizzone, S.; Trasatti, S. Interfacial properties of oxides with technological impact in electrochemistry. *Adv. Colloid Interface Sci.* **1996**, *64*, 173–251.
- (2) Gross, A.; Sakong, S. Modelling the electric double layer at electrode/electrolyte interfaces. *Curr. Opin. Electrochem.* **2019**, *14*, 1 – 6.
- (3) Adekola, F.; Fédoroff, M.; Geckeis, H.; Kupcik, T.; Lefèvre, G.; Lützenkirchen, J.; Plaschke, M.; Preočanin, T.; Rabung, T.; Schild, D. Characterization of acid-base properties of two gibbsite samples in the context of literature results. *J. Colloid Interface Sci.* **2011**, *354*, 306–317.
- (4) Zarzycki, P.; Preočanin, T. Point of zero potential of single-crystal electrode/inert electrolyte interface. *J. Colloid Interface Sci.* **2012**, *370*, 139–143.
- (5) Kosmulski, M. The pH dependent surface charging and points of zero charge. VI. Update. *J. Colloid Interface Sci.* **2014**, *426*, 209–212.
- (6) Lyons, M. E. G.; Doyle, R. L.; Browne, M. P.; Godwin, I. J.; Rovetta, A. A. S. Recent developments in electrochemical water oxidation. *Curr. Opin. Electrochem.* **2017**, *1*, 40–45.
- (7) Schmickler, W.; Santos, E. *Interfacial electrochemistry*; Springer: Berlin; London, 2010.
- (8) Nozik, A. J.; Memming, R. Physical chemistry of semiconductor-liquid interfaces. *J. Phys. Chem.* **1996**, *100*, 13061–13078.
- (9) Grätzel, M. Photoelectrochemical cells. *Nature* **2001**, *414*, 338–344.
- (10) Bolt, G. H. Determination of the Charge Density of Silica Sols. *J. Phys. Chem.* **1957**, *61*, 1166–1169.
- (11) Parks, G. A.; de Bruyn, P. L. The zero point of charge of oxides. *J. Phys. Chem.* **1962**, *66*, 967–973.
- (12) Parks, G. A. The Isoelectric Points of Solid Oxides, Solid Hydroxides, and Aqueous Hydroxo Complex Systems. *Chem. Rev.* **1965**, *65*, 177–198.
- (13) Hiemstra, T.; van Riemsdijk, W. H.; Bolt, G. H. Multisite Proton Adsorption Modeling at the Solid-Solution Interface of (Hydr)Oxides - a New Approach .1. Model Description and Evaluation of Intrinsic Reaction Constants. *J. Colloid Interface Sci.* **1989**, *133*, 91–104.
- (14) Hiemstra, T.; De Wit, J. C. M.; Van Riemsdijk, W. H. Multisite proton adsorption modeling at the solid/solution

- interface of (hydr)oxides: A new approach. II. Application to various important (hydr)oxides. *J. Colloid Interface Sci.* **1989**, *133*, –117.
- (15) Bickmore, B. R.; Tadanier, C. J.; Rosso, K. M.; Monn, W. D.; Eggett, D. L. Bond-valence methods for pKa prediction: critical reanalysis and a new approach. *Geochim. Cosmochim. Acta* **2004**, *68*, 2025–2042.
- (16) Brown, I. D. Recent Developments in the Methods and Applications of the Bond Valence Model. *Chem. Rev.* **2009**, *109*, 6858–6919.
- (17) Bickmore, B.; Rosso, K.; Mitchell, S. In *Surface Complexation Modelling*; Lajtzenkirchen, J., Ed.; Interface Science and Technology; Elsevier, 2006; Vol. 11; pp 269 – 283.
- (18) Boily, J.-F. The Variable Capacitance Model: A Strategy for Treating Contrasting Charge-Neutralizing Capabilities of Counterions at the Mineral/Water Interface. *Langmuir* **2014**, *30*, 2009–2018.
- (19) Boamah, M. D.; Ohno, P. E.; Geiger, F. M.; Eissenthal, K. B. Relative permittivity in the electrical double layer from nonlinear optics. *J. Chem. Phys.* **2018**, *148*, 222808–8.
- (20) Fujishima, A.; Honda, K. Electrochemical Photolysis of Water at a Semiconductor Electrode. *Nature* **1972**, *238*, 37–38.
- (21) Gerischer, H. Electrolytic decomposition and photodecomposition of compound semiconductors in contact with electrolytes. *J. Vac. Sci. Technol.* **1978**, *15*, 1422–1428.
- (22) Henderson, M. A. A surface science perspective on TiO₂ photocatalysis. *Surf. Sci. Rep.* **2011**, *66*, 185–297.
- (23) Pang, C. L.; Lindsay, R.; Thornton, G. Structure of Clean and Adsorbate-Covered Single-Crystal Rutile TiO₂ Surfaces. *Chem. Rev.* **2013**, *113*, 3887–3948.
- (24) Hussain, H.; Tocci, G.; Woolcot, T.; Torrelles, X.; Pang, C. L.; Humphrey, D. S.; Yim, C. M.; Grinter, D. C.; Cabailh, G.; Bikondoa, O. et al. Structure of a model TiO₂ photocatalytic interface. *Nat. Mater.* **2016**, 1–7.
- (25) Diebold, U. Perspective: A controversial benchmark system for water-oxide interfaces: H₂O/TiO₂(110). *J. Chem. Phys.* **2017**, *147*, 040901–4.
- (26) Balajka, J.; Pavelec, J.; Komora, M.; Schmid, M.; Diebold, U. Apparatus for dosing liquid water in ultrahigh vacuum. *Rev. Sci. Instrum.* **2018**, *89*, 083906–7.
- (27) Tomkiewicz, M. The Potential Distribution at the TiO₂ Aqueous Electrolyte Interface. *J. Electrochem. Soc.* **1979**, *126*, 1505–1510.
- (28) Ridley, M. K.; Hiemstra, T.; van Riemsdijk, W. H.; Machesky, M. L. Inner-sphere complexation of cations at the rutile–water interface: A concise surface structural interpretation with the CD and MUSIC model. *Geochim. Cosmochim. Acta* **2009**, *73*, 1841–1856.
- (29) Berube, Y. G.; de Bruyn, P. L. Adsorption at the rutile-solution interface. II. Model of the electrochemical double layer. *J. Colloid Interface Sci.* **1968**, *28*, 92–105.
- (30) Gerischer, H. Neglected problems in the pH dependence of the flatband potential of semiconducting oxides and semiconductors covered with oxide layers. *Electrochim. Acta* **1989**, *34*, 1005 – 1009.
- (31) Gileadi, E. Problems in interfacial electrochemistry that have been swept under the carpet. *J. Solid State Electrochem.* **2011**, *15*, 1359–1371.
- (32) Liu, L.-M.; Zhang, C.; Thornton, G.; Michaelides, A. Structure and dynamics of liquid water on rutile TiO₂(110). *Phys. Rev. B* **2010**, *82*, 161415–4.

- (33) Wesolowski, D. J.; Sofu, J. O.; Bandura, A. V.; Zhang, Z.; Mamontov, E.; Předota, M.; Kumar, N.; Kubicki, J. D.; Kent, P. R. C.; Vlcek, L. et al. Comment on "Structure and dynamics of liquid water on rutile TiO₂(110)". *Phys. Rev. B* **2012**, *85*, 167401.
- (34) Liu, L.-M.; Zhang, C.; Thornton, G.; Michaelides, A. Reply to Comment on 'Structure and dynamics of liquid water on rutile TiO₂ (110)'. *Phys. Rev. B* **2012**, *85*, 167402.
- (35) Bandura, A. V.; Kubicki, J. D.; Sofu, J. O. Periodic Density Functional Theory Study of Water Adsorption on the α -Quartz (101) Surface. *J. Phys. Chem. C* **2011**, *115*, 5756–5766.
- (36) Tocci, G.; Michaelides, A. Solvent-Induced Proton Hopping at a Water–Oxide Interface. *J. Phys. Chem. Lett.* **2014**, *5*, 474–480.
- (37) von Rudorff, G. F.; Jakobsen, R.; Rosso, K. M.; Blumberger, J. Fast Interconversion of Hydrogen Bonding at the Hematite (001)–Liquid Water Interface. *J. Phys. Chem. Lett.* **2016**, *7*, 1155–1160.
- (38) Selcuk, S.; Selloni, A. Facet-dependent trapping and dynamics of excess electrons at anatase TiO₂ surfaces and aqueous interfaces. *Nat. Mater.* **2016**, *15*, 1107–1112.
- (39) Gaigeot, M.-P.; Sprik, M.; Sulpizi, M. Oxide/water interfaces: how the surface chemistry modifies interfacial water properties. *J. Phys-Condens. Mat.* **2012**, *24*, 124106–11.
- (40) Wan, Q.; Galli, G. First-Principles Framework to Compute Sum-Frequency Generation Vibrational Spectra of Semiconductors and Insulators. *Phys. Rev. Lett.* **2015**, *115*, 246404–5.
- (41) Khatib, R.; Backus, E. H. G.; Bonn, M.; Perez-Haro, M.-J.; Gaigeot, M.-P.; Sulpizi, M. Water orientation and hydrogen-bond structure at the fluoride/water interface. *Sci. Rep.* **2016**, *6*, 24287.
- (42) Cheng, J.; Sprik, M. Acidity of the Aqueous Rutile TiO₂(110) Surface from Density Functional Theory Based Molecular Dynamics. *J. Chem. Theory Comput.* **2010**, *6*, 880–889.
- (43) Sulpizi, M.; Gaigeot, M.-P.; Sprik, M. The Silica–Water Interface: How the Silanols Determine the Surface Acidity and Modulate the Water Properties. *J. Chem. Theory Comput.* **2012**, *8*, 1037–1047.
- (44) Liu, X.; Lu, X.; Sprik, M.; Cheng, J.; Meijer, E. J.; Wang, R. Acidity of edge surface sites of montmorillonite and kaolinite. *Geochim. Cosmochim. Acta* **2013**, *117*, 180–190.
- (45) Churakov, S. V.; Labbez, C.; Pegado, L.; Sulpizi, M. Intrinsic Acidity of Surface Sites in Calcium Silicate Hydrates and Its Implication to Their Electrokinetic Properties. *J. Phys. Chem. C* **2014**, *118*, 11752–11762.
- (46) Cheng, J.; Sprik, M. Alignment of electronic energy levels at electrochemical interfaces. *Phys. Chem. Chem. Phys.* **2012**, *14*, 11245–11267.
- (47) Cheng, J.; Liu, X.; VandeVondele, J.; Sulpizi, M.; Sprik, M. Redox Potentials and Acidity Constants from Density Functional Theory Based Molecular Dynamics. *Acc. Chem. Res.* **2014**, *47*, 3522–3529.
- (48) Pham, T. A.; Ping, Y.; Galli, G. Modelling heterogeneous interfaces for solar water splitting. *Nat. Mater.* **2017**, *16*, 401–408.
- (49) Ambrosio, F.; Wiktor, J.; Pasquarello, A. pH-Dependent Catalytic Reaction Pathway for Water Splitting at the BiVO₄–Water Interface from the Band Alignment. *ACS Energy Lett.* **2018**, *3*, 829–834.

- (50) Stengel, M.; Spaldin, N. A.; Vanderbilt, D. Electric displacement as the fundamental variable in electronic-structure calculations. *Nat. Phys.* **2009**, *5*, 304–308.
- (51) Zhang, C.; Sprik, M. Computing the dielectric constant of liquid water at constant dielectric displacement. *Phys. Rev. B* **2016**, *93*, 144201.
- (52) Zhang, C.; Hutter, J.; Sprik, M. Computing the Kirkwood g-Factor by Combining Constant Maxwell Electric Field and Electric Displacement Simulations: Application to the Dielectric Constant of Liquid Water. *J. Phys. Chem. Lett.* **2016**, *7*, 2696–2701.
- (53) Zhang, C.; Sprik, M. Finite field methods for the supercell modeling of charged insulator/electrolyte interfaces. *Phys. Rev. B* **2016**, *94*, 245309.
- (54) Sayer, T.; Zhang, C.; Sprik, M. Charge compensation at the interface between the polar NaCl(111) surface and a NaCl aqueous solution. *J. Chem. Phys.* **2017**, *147*, 104702–8.
- (55) Zhang, C. Communication: Computing the Helmholtz capacitance of charged insulator-electrolyte interfaces from the supercell polarization. *J. Chem. Phys.* **2018**, *149*, 031103–6.
- (56) Sayer, T.; Sprik, M.; Zhang, C. Finite electric displacement simulations of polar ionic solid-electrolyte interfaces: Application to NaCl(111)/aqueous NaCl solution. *J. Chem. Phys.* **2019**, *150*, 041716–13.
- (57) Perdew, J. P.; Burke, K.; Ernzerhof, M. Generalized Gradient Approximation Made Simple. *Phys. Rev. Lett.* **1996**, *77*, 3865–3868.
- (58) Hutter, J.; Iannuzzi, M.; Schiffmann, F.; VandeVondele, J. CP2K:atomistic simulations of condensed matter systems. *WIREs Comput. Mol. Sci.* **2013**, *4*, 15–25.
- (59) See the Supplemental Information for the description of method and computational setup.
- (60) Limmer, D. T.; Merlet, C.; Salanne, M.; Chandler, D.; Madden, P. A.; van Roij, R.; Rotenberg, B. Charge Fluctuations in Nanoscale Capacitors. *Phys. Rev. Lett.* **2013**, *111*, 106102.
- (61) Cheng, J.; Sprik, M. The electric double layer at a rutile TiO₂ water interface modelled using density functional theory based molecular dynamics simulation. *J. Phys-Condens. Mat.* **2014**, *26*, 244108.
- (62) Parez, S.; Předota, M.; Machesky, M. Dielectric Properties of Water at Rutile and Graphite Surfaces: Effect of Molecular Structure. *J. Phys. Chem. C* **2014**, *118*, 4818–4834.
- (63) Creazzo, F.; Galimberti, D. R.; Pezzotti, S.; Gaigeot, M.-P. DFT-MD of the (110)-Co₃O₄ cobalt oxide semiconductor in contact with liquid water, preliminary chemical and physical insights into the electrochemical environment. *J. Chem. Phys.* **2019**, *150*, 041721–19.
- (64) Here we plot the supercell dipole moment M_z instead P_z where they differ just by the volume Ω of the model system $M_z = \Omega P_z$.
- (65) Junquera, J.; Cohen, M. H.; Rabe, K. M. Nanoscale smoothing and the analysis of interfacial charge and dipolar densities. *J. Phys-Condens. Mat.* **2007**, *19*, 213203.
- (66) Ong, S.; Zhao, X.; Eissenthal, K. B. Polarization of water molecules at a charged interface: second harmonic studies of the silica/water interface. *Chem. Phys. Lett.* **1992**, *191*, 327–335.
- (67) Brown, M. A.; Abbas, Z.; Kleibert, A.; Green, R. G.; Goel, A.; May, S.; Squires, T. M. Determination of Surface Potential and Electrical Double-Layer Structure at the Aqueous Electrolyte-Nanoparticle Interface. *Phys. Rev. X* **2016**, *6*, 011007–12.

- (68) Bourikas, K.; Hiemstra, T.; Van Riemsdijk, W. H. Ion Pair Formation and Primary Charging Behavior of Titanium Oxide (Anatase and Rutile). *Langmuir* **2001**, *17*, 749–756.
- (69) Hiemstra, T.; Van Riemsdijk, W. H. Physical chemical interpretation of primary charging behaviour of metal (hydr) oxides. *Colloids Surf.* **1991**, *59*, 7–25.
- (70) Yates, D. E.; Healy, T. W. Titanium dioxide–electrolyte interface. Part 2.—Surface charge (titration) studies. *J. Chem. Soc., Faraday Trans. 1* **1980**, *76*, 9–10.
- (71) Kallay, N.; Čolić, M.; Fuerstenau, D. W.; Jang, H. M.; Matijević, E. Lyotropic effect in surface charge, electrokinetics, and coagulation of a rutile dispersion. *Colloid Polym. Sci.* **1994**, *272*, 554–561.
- (72) Blok, L.; de Bruyn, P. L. The ionic double layer at the ZnO solution interface. III. Comparison of calculated and experimental differential capacities. *J. Colloid Interface Sci.* **1970**, *32*, 533–538.
- (73) Sverjensky, D. A. Prediction of surface charge on oxides in salt solutions: Revisions for 1:1 (M+L-) electrolytes. *Geochim. Cosmochim. Acta* **2005**, *69*, 225–257.
- (74) Bankura, A.; Carnevale, V.; Klein, M. L. Hydration structure of salt solutions from ab initio molecular dynamics. *J. Chem. Phys.* **2013**, *138*, 014501.
- (75) Serrano, G.; Bonanni, B.; Di Giovannantonio, M.; Kosmala, T.; Schmid, M.; Diebold, U.; Di Carlo, A.; Cheng, J.; Van deVondele, J.; Wandelt, K. et al. Molecular Ordering at the Interface Between Liquid Water and Rutile TiO₂(110). *Adv. Mater. Interfaces* **2015**, *2*, 1500246–6.
- (76) Kirkwood, J. G. The Dielectric Polarization of Polar Liquids. *J. Chem. Phys.* **1939**, *7*, 911–919.
- (77) Imanishi, A.; Fukui, K.-i. Atomic-Scale Surface Local Structure of TiO₂ and Its Influence on the Water Photooxidation Process. *J. Phys. Chem. Lett* **2014**, *5*, 2108–2117.

Coupling of Surface Chemistry and Electric Double Layer at TiO₂ Electrochemical Interfaces

Chao Zhang*, Jürg Hutter[‡] and Michiel Sprik[†]

* *Department of Chemistry-Ångström Laboratory, Uppsala University, BOX 538, 75121, Uppsala*

[‡] *Institut für Chemie, Universität Zürich, Winterthurerstrasse 190, CH-8057 Zürich*

[†] *Department of Chemistry, University of Cambridge, Lensfield Rd, Cambridge CB2 1EW*

chao.zhang@kemi.uu.se

Supporting Information

A The hybrid constant \bar{D} Hamiltonian

In this study, we used the hybrid SSV constant \bar{D} Hamiltonian which can be derived either from the thermodynamics argument originally [1] or from a current dependent Lagrangian as shown recently [2]:

$$H_D(v, \varphi, \bar{D}) = H_{\text{PBC}}(v, \varphi) + \frac{\Omega}{8\pi} (\bar{D} - 4\pi P_z(v, \varphi))^2 \quad (1)$$

where P_z is the itinerant polarization in the direction of \bar{D} (See Secs. IV B and IV C in Ref. [3] for the elaboration), which is formally defined as a time integral of the volume integral of current [4–9]. Ω is the supercell volume and $v = (\mathbf{r}^N, \mathbf{p}^N)$ are the classical degrees of freedom of a N -particle system. The electronic degrees of freedom φ_α , $\alpha = 1 \dots M$ determining the induced dipoles are collectively represented by φ . The bar over D emphasizes that it is a controllable variable instead of an observable. “Hybrid” means the field is only applied in the direction perpendicular to the surface.

In CP2K, one can switch on the hybrid constant $\bar{D} = 0$ scheme by using the following keyword block:

```
&PERIODIC_EFIELD
  INTENSITY 0.00
  DISPLACEMENT_FIELD T
  POLARISATION 0.0 0.0 1.0
  D_FILTER 0.0 0.0 1.0
&END PERIODIC_EFIELD
```

B CP2K simulations of electrified rutile TiO₂(110)-NaCl electrolyte interfaces

The electronic structure of rutile TiO₂ (110)-NaCl electrolyte systems was solved applying DFT in the Perdew-Burke-Ernzerhof (PBE) approximation [10] using CP2K suit of programs [11,

12]. Basis sets optimized for molecular systems (MOLOPT) [13] with double- ζ basis sets with one additional polarization functions (DZVP) and a charge density cutoff of 320 Ry were used. Core electrons were taken into account using the dual-space Goedecker-Teter-Hutter (GTH) pseudopotentials [14].

The model system consisted of a symmetric periodic slab of five layer O-Ti-O trilayer with (4x2) surface cell, 110 water molecules, 5 Na⁺ and 5 Cl⁻ ions in a periodic cell of 11.90 Å × 13.20 Å × 38.28 Å. To keep the composition fixed in all setups, the negatively charged side of TiO₂ slab is formed by removing H⁺ from absorbed water molecules and the positively charged side is formed by adding removed H⁺ to oxygen sites of the other side of TiO₂ slab. The integration time-step is 0.5 fs and MD trajectories were collected for about 15ps for each step-up at $\bar{D} = 0$ condition after initial equilibration at $\bar{E} = 0$ condition. The initial configuration for different charge densities were obtained from our previous work of charged insulator-electrolyte systems using a classical point-charge like model [3]. Bussi-Donadio-Parrinello thermostat [15] was used to keep the temperature at 330K throughout all simulations.

The macroscopic polarization is computed using both Resta formula [16] and maximally-localized Wannier functions (MLWFs) [17], as implemented in CP2K. This is an important technical check to ensure the branch consistency because of the multi-valued nature of the macroscopic polarization, as discussed in details in Sec. VI B in Ref. [18]. Electrostatic potential cube files were saved from CP2K every 50 fs and macro-averaging of the averaged electrostatic potential cube file was carried out using MACROAVE code [19].

References

- [1] Massimiliano Stengel, Nicola A Spaldin, and David Vanderbilt, “Electric displacement as the fundamental variable in electronic-structure calculations”, *Nat. Phys.* **5**(4), pp. 304–308 (2009).
- [2] M Sprik, “Finite Maxwell field and electric displacement Hamiltonians derived from a current dependent Lagrangian”, *Mol. Phys.* **117**, pp. 1–7 (2018).
- [3] Chao Zhang and Michiel Sprik, “Finite field methods for the supercell modeling of charged insulator/electrolyte interfaces”, *Phys. Rev. B* **94**, pp. 245309 (2016).
- [4] R D King-Smith and David Vanderbilt, “Theory of polarization in crystalline solids”, *Phys. Rev. B* **47**, pp. 1651–1653 (1993).
- [5] Raffaele Resta, “Macroscopic polarization in crystalline dielectrics: the geometric phase approach”, *Rev. Mod. Phys.* **66**, pp. 899–915 (1994).
- [6] Raffaele Resta and David Vanderbilt, “Theory of polarization: A Modern approach”, In Karin M Rabe, Charles H Ahn, and Jean-Marc Triscone, editors, *Topics in Applied Physics Volume 105: Physics of Ferroelectrics: a Modern Perspective*, pp. 31–67. Springer-Verlag (2007).
- [7] J.-M. Caillol, D Levesque, and J J Weis, “Electrical properties of polarizable ionic solutions. I. Theoretical aspects”, *J. Chem. Phys.* **91**, pp. 5544–5554 (1989).
- [8] J.-M. Caillol, D Levesque, and J J Weis, “Electrical properties of polarizable ionic solutions. II. Computer simulation results”, *J. Chem. Phys.* **91**, pp. 5555–5566 (1989).

- [9] Jean-Michel Caillol, “Comments on the Numerical Simulations of Electrolytes in Periodic Boundary Conditions”, J. Chem. Phys. **101**(7), pp. 6080–12 (1994).
- [10] John P Perdew, Kieron Burke, and Matthias Ernzerhof, “Generalized Gradient Approximation Made Simple”, Phys. Rev. Lett. **77**(18), pp. 3865–3868 (1996).
- [11] Joost VandeVondele, Matthias Krack, Fawzi Mohamed, Michele Parrinello, Thomas Chassaing, and Jürg Hutter, “Quickstep: Fast and accurate density functional calculations using a mixed Gaussian and plane waves approach”, Comput. Phys. Commun. **167**(2), pp. 103–128 (2005).
- [12] Jürg Hutter, Marcella Iannuzzi, Florian Schiffmann, and Joost VandeVondele, “cp2k:atomistic simulations of condensed matter systems”, WIREs Comput. Mol. Sci. **4**(1), pp. 15–25 (2013).
- [13] Joost VandeVondele and Jürg Hutter, “Gaussian basis sets for accurate calculations on molecular systems in gas and condensed phases”, J. Chem. Phys. **127**, pp. 114105 (2007).
- [14] S Goedecker, M Teter, and J Hutter, “Separable dual-space Gaussian pseudopotentials”, Phys. Rev. B **54**(3), pp. 1703–1710 (1996).
- [15] Giovanni Bussi, Davide Donadio, and Michele Parrinello, “Canonical sampling through velocity rescaling”, J. Chem. Phys. **126**(1), pp. 014101 (2007).
- [16] R Resta, “Quantum-mechanical position operator in extended systems”, Phys. Rev. Lett. **80**(9), pp. 1800–1803 (1998).
- [17] Nicola Marzari, Arash A Mostofi, Jonathan R Yates, Ivo Souza, and David Vanderbilt, “Maximally localized Wannier functions: Theory and applications”, Rev. Mod. Phys. **84**(4), pp. 1419–1475 (2012).
- [18] Thomas Sayer, Michiel Sprik, and Chao Zhang, “Finite electric displacement simulations of polar ionic solid-electrolyte interfaces: Application to NaCl(111)/aqueous NaCl solution”, J. Chem. Phys. **150**(4), pp. 041716–13 (2019).
- [19] Javier Junquera, Morrel H Cohen, and Karin M Rabe, “Nanoscale smoothing and the analysis of interfacial charge and dipolar densities”, J. Phys-Condens. Mat. **19**(21), pp. 213203 (2007).